PAPER • OPEN ACCESS

Rotational magic conditions for ultracold molecules in the presence of Raman and Rayleigh scattering

To cite this article: Svetlana Kotochigova *et al* 2024 *New J. Phys.* **26** 063025

IOP Publishing New J. Phys. 26 (2024) 063025 https://doi.org/10.1088/1367-2630/ad56bf

New Journal of Physics
The open access journal at the forefront of physics

Deutsche Physikalische Gesellschaft DPG
IOP Institute of Physics

Published in partnership with: Deutsche Physikalische Gesellschaft and the Institute of Physics

OPEN ACCESS

RECEIVED
16 April 2024

REVISED
27 May 2024

ACCEPTED FOR PUBLICATION
11 June 2024

PUBLISHED
20 June 2024

PAPER

Rotational magic conditions for ultracold molecules in the presence of Raman and Rayleigh scattering

Svetlana Kotochigova[1,*], Qingze Guan[1,2], Eite Tiesinga[3], Vito Scarola[4], Brian DeMarco[5] and Bryce Gadway[5]

[1] Department of Physics, Temple University, Philadelphia, PA 19122, United States of America
[2] Department of Physics and Astronomy, Washington State University, Pullman, WA 99164-2814, United States of America
[3] Joint Quantum Institute, National Institute of Standards and Technology and the University of Maryland, Gaithersburg, MD 20899, United States of America
[4] Department of Physics, Virginia Tech, Blacksburg, VA 24061, United States of America
[5] Department of Physics and IQUIST, University of Illinois at Urbana-Champaign, Urbana, IL 61801-3080, United States of America
[*] Author to whom any correspondence should be addressed.

E-mail: skotoch@temple.edu

Keywords: ultracold molecules, Raman and Rayleigh scattering, magic trapping conditions, superpositions of multiple rotational states

Abstract

Molecules have vibrational, rotational, spin-orbit and hyperfine degrees of freedom or quantum states, each of which responds in a unique fashion to external electromagnetic radiation. The control over superpositions of these quantum states is key to coherent manipulation of molecules. For example, the better the coherence time the longer quantum simulations can last. The important quantity for controlling an ultracold molecule with laser light is its complex-valued molecular dynamic polarizability. Its real part determines the tweezer or trapping potential as felt by the molecule, while its imaginary part limits the coherence time. Here, our study shows that efficient trapping of a molecule in its vibrational ground state can be achieved by selecting a laser frequency with a detuning on the order of tens of GHz relative to an electric-dipole-forbidden molecular transition. Close proximity to this nearly forbidden transition allows to create a sufficiently deep trapping potential for multiple rotational states without sacrificing coherence times among these states from Raman and Rayleigh scattering. In fact, we demonstrate that magic trapping conditions for multiple rotational states of the ultracold ^{23}Na^{87}Rb polar molecule can be created.

1. Introduction

Electro-magnetic radiation plays a central role in the trapping and detection of ultracold molecules as well as the control of superpositions of their internal rovibrational and even external motional states. Some early highlights in trapping and state preparation for molecules can be found in references [1–4]. Optical tweezers and optical lattices, focused and retero-reflected laser beams in the near infra-red or optical frequency domain, are the modern tools to trap molecules. For polar diatomic molecules, a natural choice for building a molecular quantum computer, qubits are formed by pairs of rotational levels of their ground vibrational state. Electric dipole–dipole interactions between such heteronuclear molecules lead to entanglement and are important for simulating many-body Hamiltonians. To make appropriate use of molecular rotation we must avoid dephasing due to light-induced rotational coupling. This may be achieved by choosing 'magic' trapping conditions. In such traps, light-induced energy shifts of two or more rotational states are identical, eliminating dephasing associated with spatial variations in intensity across the trap. Recently, this was achieved with heteronuclear alkali-metal dimers [5–7].

The guiding principles of selecting trapping laser frequencies for ultracold ground-state molecules are to choose the frequency either well below the minimum energy of the electronically excited potentials or in the near-resonant region of mostly forbidden molecular transitions. The first idea was realized in multiple experiments using YAG lasers with wavelengths around 1064 nm [2, 5, 8]. These studies with off-resonant light have also shown that magic conditions can only exist as long as the angles between the laser polarization

and either the direction of an external static magnetic or electric field are carefully controlled. In fact, the authors of reference [2] showed in measurements of the AC polarizability and of the coherence time of microwave transitions between rotational states that there exists an optimal angle between the orientation of the light polarization and a magnetic field.

The second approach for the construction of rotational magic traps was pioneered for ^{23}Na^{40}K [9], ^{87}Rb^{133}Cs [6, 10], and ^{23}Na^{87}Rb [7, 11]. In all cases, the authors used a laser with a carefully chosen frequency between two vibrational levels of the excited $b^3\Pi_{0^+}$ molecular electronic state. Electric dipole transitions from the ground $X^1\Sigma^+$ state to this electronic state are narrow and almost forbidden. The laser detuning from vibrational levels is relatively small on the order of tens of GHz. Most importantly, external electric or magnetic fields are not required. Nevertheless, this second approach can be readily applied to related diatomic and polyatomic molecules.

This paper describes quantitative theoretical calculations aimed at finding 'magic' conditions for ultracold ^{23}Na^{87}Rb molecules prepared in superpositions of rotational states of its vibrational ground state and held in place by tweezer forces. We focus on the second approach using a frequency region just above the minimum of the potential of the exited $b\,^3\Pi_{0^+}$ molecular state in the presence of a 335 G magnetic field defining a natural quantization direction. This magnetic field strength, corresponding to the field location of a Fano–Feshbach resonance in the collision of ultracold ^{23}Na and ^{87}Rb atoms, was inspired by the experiments described in [12]. No electric field is present and the polarization of the tweezer light is linear and along the magnetic field direction contrasting with the conditions studied in [7]. We have also developed an approach to enhance coherence times for superpositions of more than two rotational states and derive approximate analytical expressions for the dynamic polarizabilities in order to better understand the origin of magic conditions. These expressions will enable experimentalists to analyze magic conditions for their own molecular system and experimental conditions.

Unavoidable scatter of photons out of laser beams by a molecule leads to detrimental off-resonant scattering and decoherence. The relevant processes are then classified as either Raman or Raleigh scattering. In both processes scattering corresponds to the off-resonant absorption of a laser photon by the molecule, promoting the molecule to an electronically excited state, followed by spontaneous emission of a photon into a bath mode. In this paper, we determine rates for molecular Raman and Rayleigh photon-scattering processes corresponding to the stimulated absorption of a laser photon by the molecule, promoting the molecule to an electronically excited state, followed by spontaneous emission of a photon. For Raman scattering the initial and final rovibrational molecular states are different whereas for Rayleigh scattering the initial and final state are the same. These processes define the ultimate limit on coherence times. For laser-cooled atoms, these scattering processes were studied in [13–15]. In this paper, we give for the first time guidance to experimentalists on how to minimize all or parts of these decoherence processes for heteronuclear molecules.

2. Magic trapping frequencies near $b^3\Pi_{0^+}$, $v' = 0$ rotational resonances

We begin by calculating the dynamic polarizability or AC Stark shift $\alpha_{X,vJM}(\nu,\vec{\varepsilon})$ for rotational levels $J = 0$ to 5 of the $v = 0$ vibrational level $|X, vJM\rangle$ of the ground $X^1\Sigma^+$ state of the ^{23}Na^{87}Rb molecule in the absence of external electric or magnetic fields and without molecular spin-rotation, hyperfine, and Zeeman interactions. Here, M is the projection quantum number of angular momentum J along a laboratory or space-fixed axis to be defined later. The tweezer laser with laser frequency ν is linearly polarized along space-fixed direction $\vec{\varepsilon}$ throughout this paper. We then determine laser light frequencies that allow simultaneous magic trapping of multiple rotational states using light nearly resonant with rovibrational levels of the $b^3\Pi_{0^+}$ electronic state. Transitions between the $X^1\Sigma^+_{0^+}$ and $b^3\Pi_{0^+}$ states are weak and only allowed through weak spin–orbit coupling with the $A^1\Sigma^+_{0^+}$ state. See [16] for a description of molecular notation.

Figure 1(a) schematically shows the NaRb molecule trapped in a tweezer potential, while figure 1(b) displays the three relevant relativistic Hund's case (c) $\Omega^\sigma = 0^+$ potential energy curves of the NaRb molecule, where Ω is the absolute value of the projection quantum number of the total electronic angular momentum along the internuclear axis and $\sigma = \pm$ represents the symmetry of $\Omega = 0$ electronic wavefunctions under reflection through a plane containing the internuclear axis. More precisely, the excited non-relativistic Hund's case (a) $A^1\Sigma^+_{0^+}$ and $b^3\Pi_{0^+}$ states are coupled by the spin-orbit interaction, which leads to two relativistic $\Omega = 0^+$ adiabatic potentials that have a narrow avoided crossing near interatomic separation $R \approx R_c = 7.5a_0$ [17], where $a_0 = 0.0529$ nm is the Bohr radius. The energetically lowest $\Omega = 0^+$ rovibrational states near the bottom or minimum of the nominally $b^3\Pi_{0^+}$ potential have a small admixture of the $A^1\Sigma^+_{0^+}$ state. As electric dipole transitions between the singlet $X^1\Sigma^+$ and triplet $b^3\Pi_{0^+}$ states are forbidden, this leads to weak, but easily observable transitions from rovibrational levels of the $X^1\Sigma^+$, $\Omega = 0^+$ state. We observe that the equilibrium separations and harmonic frequencies of the $X^1\Sigma^+$ and $b^3\Pi_{0^+}$ states

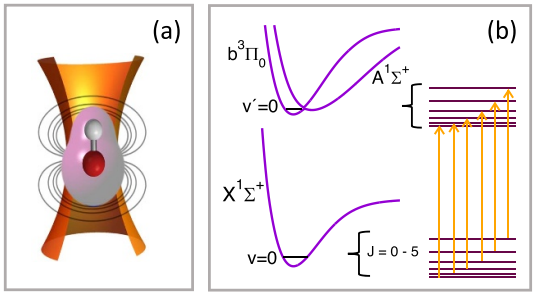

Figure 1. (a) Schematic presentation of ground-state heteronuclear NaRb trapped in an optical tweezer potential. (b) The potential energies (purple curves) as function of atomic separation of the three most-important for us electronic states of NaRb. The two black horizontal lines in the potentials represent the energetically lowest $v = 0$ and $v' = 0$ vibrational levels of the $X^1\Sigma^+$ state and the coupled $A^1\Sigma^+$ and $b^3\Pi_{0+}$ complex, respectively. Relevant rotational levels $J = 0$ to 5 for both of these vibrational states are shown on the right. Near resonant optical transitions, orange lines with arrows, are used in a search for magic conditions as a function of tweezer laser frequency.

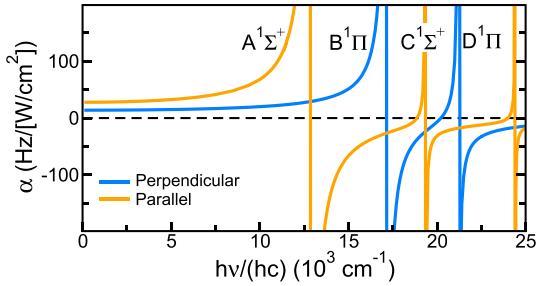

Figure 2. The quasi-static parallel (orange curve) and perpendicular (blue curve) electronic polarizabilities of the $X^1\Sigma^+$ state at its equilibrium separation $R_e = 6.885a_0$ and photon energies up to $hc \times 25\,000\,\mathrm{cm}^{-1}$. The energetically lowest four resonances are labeled with state $^1\Lambda$. The data is based on non-relativistic configuration-interaction calculations with the Q-Chem software package.

are almost the same. We have used the non-relativistic $X^1\Sigma^+$, $A^1\Sigma^+_{0+}$ and $b^3\Pi_{0+}$ potentials, spin-orbit matrix elements, and the $X^1\Sigma^+$ to $A^1\Sigma^+$ electronic transition dipole moment as functions of R given by [17, 18].

For rotational states J, M of the $v = 0$ $X^1\Sigma^+$ ground-state of NaRb, the calculation of the sum over intermediate, excited states that appears in the evaluation of $\alpha_{X,vJM}(\nu, \vec{\varepsilon})$ can be simplified. The relevant laser frequencies are *nearly resonant* with rovibrational levels near the minimum of the $b^3\Pi_{0+}$ potential. Consequently, we write $\alpha_{X,vJM}(\nu, \vec{\varepsilon}) = \alpha_{\mathrm{res}}(\nu, \vec{\epsilon}) + \alpha_{\text{off- res}}(\nu, \vec{\epsilon})$. The first contribution $\alpha_{\mathrm{res}}(\nu, \vec{\epsilon})$ corresponds to the polarizability due to the energetically lowest and thus *near-resonant* ro-vibrational states of the $A^1\Sigma^+$ and $b^3\Pi_{0+}$ complex. A second contribution $\alpha_{\text{off- res}}(\nu, \vec{\epsilon})$ corresponds to *off-resonant* transitions to other electronic states. The latter contribution is computed within a quasi-static approximation, where so-called parallel and perpendicular polarizabilities $\alpha_{\parallel}(\nu, R)$ and $\alpha_{\perp}(\nu, R)$, corresponding to laser polarizations parallel and perpendicular to the body-fixed internuclear axis, respectively, are computed as functions of laser frequency ν and atom-atom separation R near the equilibrium separation R_e of the $X^1\Sigma^+$ state using the linear response theory formulation within software package Q-Chem [19]. Q-Chem computes electronic states based on a non-relativistic description of the electrons. In practice, we realize that these two quasi-static polarizabilities are to good approximation independent of R over the radial width of the $v = 0$ vibrational level of the $X^1\Sigma^+$ state. We thus only compute $\alpha_{\parallel}(\nu, R)$ and $\alpha_{\perp}(\nu, R)$ at $R = R_e$ and drop argument R for the remainder of this article.

The two quasi-static polarizabilities of the $X^1\Sigma^+$ state have been obtained with a non-relativistic configuration-interaction electronic-structure calculation using an all-electron basis set for Na. Single and double excitations were allowed from these basis functions. An effective core potential describes the 28 inner electrons of Rb. Single and double excitations from electron shells $4s^2 4p^6 5s$ were allowed for the remaining nine electrons of Rb.

Figure 2 shows the two quasi-static polarizabilities of the $X^1\Sigma^+$ state of NaRb at $R = R_e$ as functions of photon energy up to $hc \times 25\,000\,\mathrm{cm}^{-1}$. Here, h is the Planck constant and c is the speed of light in vacuum. Over this large photon-energy range, several resonances are visible. Each corresponds to a transition between the $X^1\Sigma^+$ state and a $^1\Lambda$ state. In fact, in our non-relativistic formulation, $\alpha_{\parallel}(\nu)$ only contains contributions

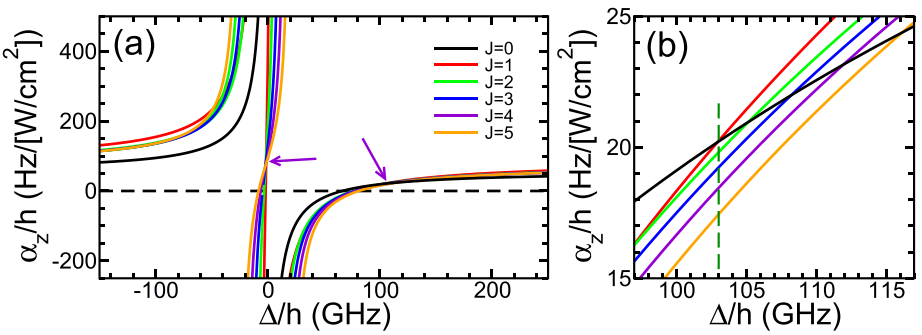

Figure 3. (a) ^{23}Na^{87}Rb dynamic polarizabilities of rotational levels of the $v=0$ $X^1\Sigma^+$ state in atomic units for z-linear polarized light as functions of laser frequency detuning Δ/h near transitions from the $v=0$ $X^1\Sigma^+$ state to the $v'=0$ level of the coupled $A^1\Sigma^+$-$b^3\Pi_{0^+}$ system. Each curve corresponds to the dynamic polarizability of a different rotational level J with $M=0$. Zero detuning Δ corresponds to the resonant transition from $v=0$, $J=0$ level of the $X^1\Sigma^+$ state to the $v'=0, J'=1$ level of the coupled $A^1\Sigma^+$-$b^3\Pi_{0^+}$ system. The purple arrows indicate magic detunings, where rotational states have the same or nearly the same polarizabilities. (b) Magnified region of dynamic polarizabilities near frequency detuning $\Delta/h=103$ GHz, where $J=0$ and 1 rotational states are magic. The colors of the curves are the same as those in panel (a).

from transitions to singlet $^1\Sigma^+$ electronic states, while $\alpha_\perp(\nu)$ only contains contributions from transitions to singlet $^1\Pi$ states.

The resonant contribution to the polarizability has been determined in several steps. We compute two-channel radial eigenvalues and eigenfunctions of the spin-orbit coupled and shifted $\Omega=0^+$ $A^1\Sigma^+$ and $b^3\Pi_{0^+}$ states for total angular momentum $J'=0, 1, \ldots, 6$ using a discrete variable representation (DVR) of the radial relative kinetic energy operator [20]. For each J', the eigenvalues $E_{\mathrm{Ab},v'J'}$ are labeled $v'=0, 1, \ldots$ with increasing energy and wavefunctions of the energetically lowest v' levels are to good approximation $b^3\Pi_{0^+}$ states. The eigenenergies are independent of projection quantum number M' of J'.

We then compute vibrational wavefunctions and energies $E_{\mathrm{X},vJ}$ of the $X^1\Sigma^+$ state for J up to 5 with the same DVR and radial grid used to compute eigenpairs of the coupled $A^1\Sigma^+$ and $b^3\Pi_{0^+}$ system. The eigenenergies are independent of projection quantum number M of J. The use of the same radial grid avoids interpolation of wavefunctions in the computation of vibrationally-averaged transition dipole moments using the R-dependent transition dipole moment between the $X^1\Sigma^+$ and $A^1\Sigma^+$ states.

Finally, we compute the resonant-part of the polarizability $\alpha_{\mathrm{X},vJM}(\nu,\vec{\varepsilon})$ of $v=0, JM$ $X^1\Sigma^+$ states using only the energetically lowest rovibrational levels of the coupled $A^1\Sigma^+$-$b^3\Pi_{0^+}$ system that have a large $b^3\Pi_{0^+}$ character and thus a small vibrationally-averaged transition dipole moment. The choice to limit the determination of the resonant-part of the polarizability to a few levels of the $A^1\Sigma^+$-$b^3\Pi_{0^+}$ system avoids double counting the effects of the $A^1\Sigma^+$ state when combining the resonant and off resonant contributions of $\alpha_{\mathrm{X},vJM}(\nu,\vec{\varepsilon})$. In principle, the M projection degeneracy is broken by the Zeeman interactions for the nuclear spins combined with quadrupolar hyperfine interactions between the nuclear quadrupole moments and the rotation of the molecule. The nuclear spin of both ^{23}Na and ^{87}Rb is 3/2. Hyperfine splittings for $\Omega=0^+$ states, as shown in reference [12], are small compared to the rotational energies described below. Moreover, nuclear Zeeman shifts at a few hundred Gauss, as will be studied here, are larger than the splittings induced by the quadrupolar hyperfine interactions and especially for the larger rotational states J as the strength of the quadrupolar hyperfine interactions scale as $1/\sqrt{J}$. Hence, we omit the effects of quadrupole hyperfine interactions on the magic conditions.

Figure 3 shows dynamic polarizabilities of the $v=0$, $J=0$, 1,…, 5 rotational levels of the ^{23}Na^{87}Rb $X^1\Sigma^+$ state with projection quantum number $M=0$ in a 335 Gauss magnetic field parallel to the polarization of linearly polarized light as functions of laser frequency in the neighborhood of the $v'=0$ level of the coupled $A^1\Sigma^+$-$b^3\Pi_{0^+}$ system. There is no external electric field applied. The dynamic polarizabilities include both resonant and off-resonant contributions and we chose the quantization axis of the molecular angular momentum J and J' in the same direction as that of the laser polarization. The horizontal axis gives photon energy detuning $\Delta=h\nu-\mathcal{E}_{v'=0}$, where molecular transition energy $\mathcal{E}_{v'=0}=E_{\mathrm{Ab},v'=0,J'=1}-E_{\mathrm{X},v=0,J=0}$. Our estimate provides that $\mathcal{E}_{v'=0}=hc\times 11\,306.1$ cm^{-1}, which corresponds to a laser wavelength close to 884.6 nm. These results are in a good agreement with the experimental measurements and theoretical calculations of reference [7].

The curves for $J=0$ and $J>0$ in figure 3 have different behaviors. The polarizability for the $J=0$ has a single resonance at $\Delta=0$. Those for $J>0$ have two resonances located at $L_J(v=0,v'=0)$ and $R_J(v=0,v'=0)$, respectively, where

$$L_J(v,v') = J(J+1)\,B_v - [J(J-1)-2]\,B_{v'} \tag{1}$$

for $J'=J-1$ and

$$R_J(v,v') = J(J+1)\,B_v - [(J+1)(J+2)-2]\,B_{v'} \tag{2}$$

for $J'=J+1$ with rotational constants B_v and $B_{v'}$ for the v vibrational level of the $X^1\Sigma^+$ state and the v' vibrational level of the coupled $A^1\Sigma^+$-$b^3\Pi_{0^+}$ system, respectively. For $^{23}Na^{87}Rb$, $B_{v=0}/hc = 0.069\,70\ \mathrm{cm}^{-1}$ and $B_{v'=0}/hc = 0.069\,88\ \mathrm{cm}^{-1}$. The two values agree to better than 0.5 %. These Equations follow from photon selection rules $|J-1|\leqslant J'\leqslant J+1$ and $|J'-J|$ is odd.

Panel (a) of figure 3 shows that there exist two *magic* laser frequencies. The first is located near $\Delta/h=-2$ GHz and $J>0$ rotational levels have nearly the same polarizabilities. The polarizability for $J=0$ is large and positive at this detuning. The second is located near $\Delta/h=+100$ GHz, all $J=0,\ldots,5$ rotational levels have nearly the same polarizabilities. The value of the polarizability at these magic frequencies leads to trap depths divided by the Planck constant on the order of tens of kHz at reasonable laser intensities of order kW cm^{-2}. Panel (b) looks in more detail at the latter frequency region. In particular, the polarizabillity of the $J=0$ level is equal to that of the $J=1$, 2, 3, 4, 5 rotational levels at detuning $\Delta/h=103$ GHz, 105 GHz, 108 GHz, 112 GHz, and 116 GHz, respectively. In fact, the differences between these Δ with $J>0$ is increasing with J. The origin of this effect lies in the quadratic increase of rotational energies with J.

3. Analytical results for magic polarizability

We find it useful to derive analytical expression for the dynamic polarizabilities shown in Figure 3 in order to better understand the origin of magic conditions as well as simplifying their determination for wide variety of molecules. In [6] we already presented an analytic approximation for the magic conditions of rotational states with projection quantum number $M=0$ in the RbCs molecule. Here, we expand our derivations to any value of M.

For rovibrational level $v=0$ JM of the $X^1\Sigma^+$ state, the dynamic polarizability for linearly-polarized laser light near transitions to vibrational states $v'=0$ or $v'=1$ of the coupled $A^1\Sigma^+$-$b^3\Pi_{0^+}$ system is well approximated by

$$\begin{aligned}\alpha_{X,v=0JM}(\nu,\vec{\varepsilon}) = &-\frac{3\pi c^2}{2\omega_{v'}^3}\left[A_{J,M}(\theta_\mathrm{p})\,\frac{\hbar\Gamma_{0,v'}}{\Delta_{v'}+L_J(0,v')}+B_{J,M}(\theta_\mathrm{p})\,\frac{\hbar\Gamma_{0,v'}}{\Delta_{v'}+R_J(0,v')}\right]\\ &+\left[A_{J,M}(\theta_\mathrm{p})+B_{J,M}(\theta_\mathrm{p})\right](\alpha_{\mathrm{bg},\parallel}-\alpha_{\mathrm{bg},\perp})+\alpha_{\mathrm{bg},\perp}\,,\end{aligned} \tag{3}$$

where θ_p is the angle between the polarization of the laser $\vec{\varepsilon}$ with respect to the quantization axis for the molecular states, our laboratory-fixed z axis. The energy detuning

$$\Delta_{v'} = h\nu - \hbar\omega_{v'} \tag{4}$$

with $\hbar\omega_{v'} = E_{\mathrm{Ab},v',J'=1} - E_{\mathrm{X},v=0,J=0}$. The terms on the first two lines of equation (3) lead to resonances in the dynamic polarizability. In fact, there are one and two resonances for $J=0$ and $J>0$, respectively. The $\Gamma_{0,v'}$ are linewidths of the vibrational levels v' of the coupled $A^1\Sigma^+$-$b^3\Pi_{0^+}$ system.

The parallel and perpendicular $\alpha_{\mathrm{bg},\parallel}$ and $\alpha_{\mathrm{bg},\perp}$ are body-fixed background polarizabilities. The dimensionless angular factor $A_{J,M}(\theta_\mathrm{p})$ is given by

$$A_{J,M}(\theta_\mathrm{p}) = \tfrac{J(J+1)-3M^2}{2(2J+1)(2J-1)}\cos^2\theta_\mathrm{p} + \tfrac{(J-1)J+M^2}{2(2J+1)(2J-1)} \tag{5}$$

for $|M|<J$ and

$$A_{J,M}(\theta_\mathrm{p}) = \frac{J}{2(2J+1)}\sin^2\theta_\mathrm{p} \tag{6}$$

for $|M|=J$. Note that $A_{J,M}(\theta_\mathrm{p})=0$ for $J=0$. Finally, the dimensionless $B_{J,M}(\theta_\mathrm{p})$ is given by

$$B_{J,M}(\theta_\mathrm{p}) = \tfrac{J(J+1)-3M^2}{2(2J+1)(2J+3)}\cos^2\theta_\mathrm{p} + \tfrac{(J+1)(J+2)+M^2}{2(2J+3)(2J+1)}\,. \tag{7}$$

Equation (3) can only be used for energy detunings that are much smaller than the vibrational spacing between different v' states of the $A^1\Sigma^+$-$b^3\Pi_{0+}$ system. On the other hand, the energy detunings must be much larger than any hyperfine and Zeeman splittings in the coupled $A^1\Sigma^+$-$b^3\Pi_{0+}$ system and for energy detunings much larger than $\hbar\Gamma_{0,v'}$.

Finally, a Taylor expansion of the right hand side of equation (3) assuming $|\Delta_{v'}| \gg |L_J|$ and $|\Delta_{v'}| \gg |R_J|$ gives

$$\alpha_{X,v=0JM}(\nu,\vec{\varepsilon}) = \left[A_{J,M}(\theta_p) + B_{J,M}(\theta_p)\right]\left(-\frac{3\pi c^2}{2\omega_{v'}^3}\frac{\hbar\Gamma_{0,v'}}{\Delta_{v'}} + \alpha_{bg,\parallel} - \alpha_{bg,\perp}\right) + \alpha_{bg,\perp}, + \cdots . \tag{8}$$

From an inspection of equation (8), we realize that we can always find an energy detuning independent of θ_p and J such that the term in parenthesis vanishes. At this energy detuning the dynamic polarizability is $\alpha_{bg,\perp}$, the same for all θ_p and J within our approximations, and the optical trap is magic for all rotational states. Higher-order terms in equation (8) will add small θ_p- and J-dependent corrections and are observed in figure 3.

4. Vibrationally-resolved imaginary polarizabilities of the $X^1\Sigma^+$ state

In addition, we use the expressions in references [1] to evaluate the imaginary dynamic polarizabilities of rovibrational levels of the ground state in vicinity of rovibrational levels of the excited state potentials. The imaginary part of α_i describes incoherent decay that leads to loss of molecules from the optical trap. Our calculation is based on perturbation theory method with specific focus on relativistic spin–orbit coupling between $A^1\Sigma^+$-$b^3\Pi_0$ complex. The simulations are performed using electronic potentials, permanent, and transition dipole moments of NaRb determined in references [17, 18, 21].

The molecular dynamic polarizability $\alpha_i(h\nu,\vec{\epsilon})$ at frequency ν and laser polarization $\vec{\epsilon}$ of state i is complex valued. To good approximation its imaginary part is

$$\mathrm{Im}\left[\alpha(h\nu,\vec{\epsilon})\right] = -\frac{1}{\epsilon_0 c}\sum_f \frac{\hbar\gamma_f/2}{\left(E_f-E_i\right)^2-(h\nu)^2}\left|\langle f|d(R)\,\hat{R}\cdot\vec{\epsilon}\,|i\rangle\right|^2, \tag{9}$$

where kets $|i\rangle$ and $|f\rangle$ are simplified labels for initial rovibrational wavefunctions of the $X^1\Sigma^+$ potential and those of excited electronic states, respectively. Their energies are E_i and E_f, respectively, and γ_f is the natural line width of excited rovibrational levels. By construction, the imaginary part is negative.

We evaluated the rovibrational molecular line widths of excited electronic states dissociating to either a singly-excited Na or Rb atom by first computing a R-dependent optical potential $-i\Gamma(R)/2$ [22] for each excited electronic state. Here, $\Gamma(R)$ is positive and proportional to $|\delta V(R)|^3 d^2(R)$, where $\delta V(R)$ and $d(R)$ at internuclear separation R are the potential energy difference and the transition electronic dipole moment between an excited state and the ground state, respectively. Finally, the energies E_i and E_f and line widths γ_f of rovibrational levels of electronic states were found by computing radial rovibrational wavefunctions, energies, and matrix elements of $\Gamma(R)$.

Figures 4(a), (b), and (c) show imaginary dynamic polarizabilities for the $J=0$, 1, and 2 rotational levels of the $v=0$ $X^1\Sigma^+$ state, respectively, as functions of laser photon energies between $hc\times 5000\,\mathrm{cm}-1$ and $hc\times 20000\,\mathrm{cm}^{-1}$. The rotational projection quantum number is $M=0$. We observe resonances from vibrational levels of the multiple excited state potentials. It turns out that, to good approximation, the three curves are the same except for a frequency-independent scale factor. Deviations from these scalings occur very close to the resonances, i.e. on the order of the rotational spacing of the molecule. The imaginary part is seven orders of magnitude smaller than the real part. For $J=1$ and 2, $M=0$ the polarizability depends on the polarization direction of the trapping light.

The imaginary parts of the polarizabilities are slowly varying with frequency in regions outside multiple closely spaced resonant features, where $\alpha(h\nu,\vec{\epsilon})$ is orders of magnitude larger than in the slowly varying regions. The resonant like features are due to the rovibrational bound states of excited electronic potentials. In fact, we could assign the resonances as due to the $b^3\Pi$, $A^1\Sigma^+$, and $B^1\Pi$ states. These resonances are strongest when the inner- or outer-turning point of rovibrational wavefunctions of the excited electronic potentials coincides with the equilibrium separation of the $X^1\Sigma^+$ potential.

The calculations of the imaginary part of the polarizability allowed us predict the role of unwanted decoherence processes. In particular, optical fields can transfer population from a rovibrational level of the electronic ground state to rovibrational levels of an excited electronic state, which then by the spontaneous emission decays to many rovibrational levels of the $X^1\Sigma^+$ state. As a result, we lose control over the molecule.

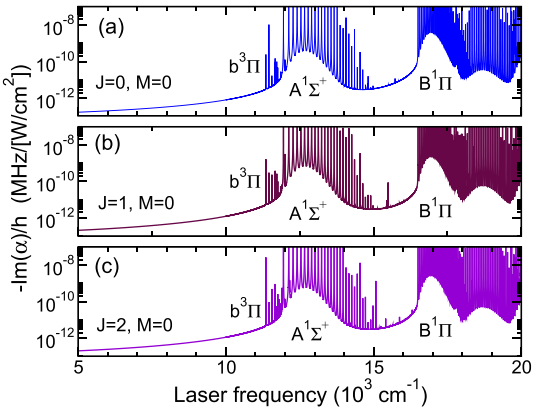

Figure 4. Minus one times the imaginary part of the dynamic polarizabilities of the $J = 0$, 1, and 2 rotational levels of the vibrational ground state of ^{23}Na^{87}Rb with projection quantum number $M = 0$ along the z axis as functions of laser frequency in panels (a), (b), and (c), respectively. Imaginary polarizabilities are presented for laser polarization σ_s along the $\hat{z}$ direction.

5. Effect of Raman and Rayleigh scattering on the magic conditions

Spontaneous photon scatter after the absorption of an optical laser photon leads to loss of information about the ro-vibrational state of the $X^1\Sigma^+$ molecule as scattered photons remain undetected. Two processes can occur. For Raman scattering the initial vJM and final $v'J'M'$ ro-vibrational levels of the $X^1\Sigma^+$ molecular state have a different energy. For Raleigh scattering the initial and final state have the same energy and the spontaneously-emitted photon only differs in direction from that of the absorbed laser photon.

The rate for Raman and Rayleigh processes is proportional to the square of a sum of two-photon transition amplitudes and inteferences play a prominant role [13, 14]. Following the derivations in [13, 14, 23] in SI units the state-to-state *off-resonant* decay rate is

$$\begin{aligned}\gamma_{\mathrm{X},v'J'M'\leftarrow\mathrm{X},vJM} &= n_\nu\, c\,\sigma_{\mathrm{X},v'J'M'\leftarrow\mathrm{X},vJM}\\ &= \frac{\sigma_{\mathrm{X},v'J'M'\leftarrow\mathrm{X},vJM}}{h\nu}\, I\end{aligned} \tag{10}$$

with laser-photon number density n_ν of photons with energy $h\nu$ and polarization ϵ, and laser intensity $I = h\nu n_\nu c$. Moreover, the state-to-state resolved cross section

$$\sigma_{\mathrm{X},v'J'M'\leftarrow\mathrm{X},vJM} = \frac{8\pi}{3}\alpha^4 a_0^2 \frac{h\nu\,(h\nu')^3}{E_\mathrm{h}^4}|\mathcal{G}|^2\,, \tag{11}$$

where α is the fine structure constant, E_h is the Hartree energy, and dimensionless

$$\begin{aligned}|\mathcal{G}|^2 = \frac{E_\mathrm{h}}{(ea_0)^2}\sum_{q=-1}^{1}\Bigg|\sum_{e,v''J''M''}\Bigg[&\frac{\langle \mathrm{X},v'J'M'|d_q|e,v''J''M''\rangle\langle e,v''J''M''|\vec{d}\cdot\vec{\epsilon}|\mathrm{X},vJM\rangle}{E_{\mathrm{X},vJM}+h\nu-E_{e,v''J''M''}}\\ &+\frac{\langle \mathrm{X},v'J'M'|\vec{d}\cdot\vec{\epsilon}|e,v''J''M''\rangle\langle e,v''J''M''|d_q|\mathrm{X},vJM\rangle}{E_{\mathrm{X},vJM}-E_{e,v''J''M''}-h\nu'}\Bigg]\Bigg|^2\,,\end{aligned} \tag{12}$$

where $h\nu' = E_{e,v''J''} - E_{\mathrm{X},v'J'}$ is the energy of the spontaneously emitted photon, $E_{\mathrm{X},v'J'M'} - E_{\mathrm{X},vJM} \leqslant h\nu$, and operator d_q is the R-dependent transition electronic dipole moment. The sum inside the absolute value is over all rovibrational levels and continuum states $v''J''M''$ of electronically excited states e. In practice, for pair M and M' and $\vec{\epsilon} = \hat{z}$ only one projection q contributes in the sum over q and the second term in the square brackets is negligible for laser frequencies in the optical domain.

In figure 5 we plot three contributions to the Raman scattering rate summed over final state M' projection, $\sum_{M'}\gamma_{\mathrm{X},v'J'M'\leftarrow\mathrm{X},vJM}$, for the $v = 0, J = 0$ (and thus $M = 0$) rovibrational level of the $X^1\Sigma^+$ state of ^{23}Na^{87}Rb as functions of laser frequency. The sum of the three contributions corresponds to the total Raman scattering rate for this state. Two of the three contributions have a resonant Fano line profile with a large value at the transition energy between the $v = 0, J = 0$ $X^1\Sigma^+$ level and the $v'' = 0, J'' = 1$ level of the coupled $A^1\Sigma^+$-$b^3\Pi_0$ system and a very small value to the blue of this transition. The $\mathrm{X}, v = 0, J = 0 \rightarrow \mathrm{X}, v' = 0, J' = 1$ contribution does not have a resonance and is constant over the range of

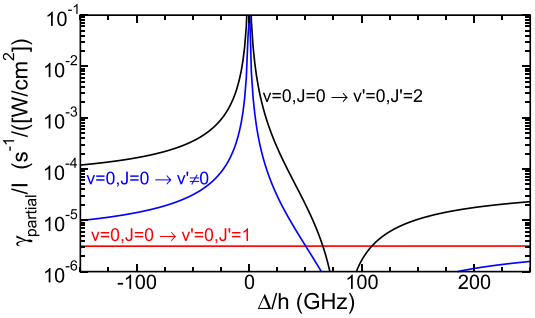

Figure 5. Contributions to the Raman scattering rate divided by laser intensity, $\gamma_{\rm partial}/I$, of the $v=0, J=0$ rovibrational level of the $X^1\Sigma^+$ state of $^{23}Na^{87}Rb$ as functions of laser frequency detuning Δ/h from the $v''=0, J''=1$ level of the coupled $A^1\Sigma^+$-$b^3\Pi_0$ system. The red, black, and blue curves correspond to contributions to final rovibrational levels $(v'=0, J'=1)$, $(v'=0, J'=2)$, and $v'\neq 0$ of the $X^1\Sigma^+$ state, respectively. The laser is linearly polarized.

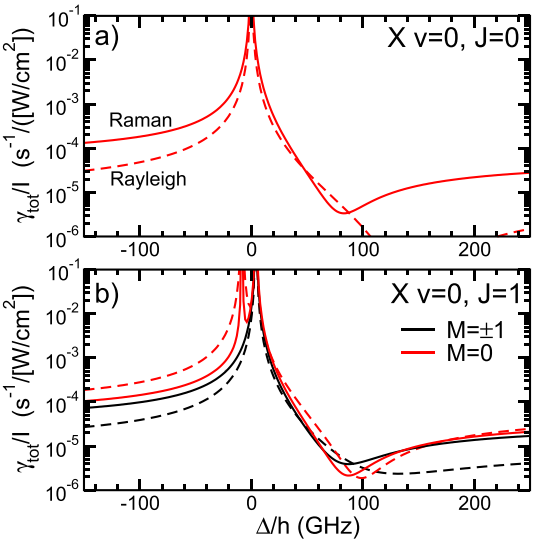

Figure 6. Total Raman and Rayleigh scattering rates divided by laser intensity, $\gamma_{\rm tot}/I$, of the $v=0, J=0, M=0$ (panel (a)) and $v=0, J=1, M=\pm1, 0$ (panel (b)) rovibrational levels of the $X^1\Sigma^+$ state of $^{23}Na^{87}Rb$ as functions of laser frequency detuning Δ/h from the $v=0, J=0$ $X^1\Sigma^+$ state to the $v''=0, J''=1$ level of the coupled $A^1\Sigma^+$-$b^3\Pi_0$ system. The solid and dashed curves in both panels correspond to Raman and Rayleigh scattering, respectively. In panel (b) black and red curves correspond to rates for levels with projection quantum numbers $|M|=1$ and $M=0$, respectively. The laser is linearly polarized along the space-fixed quantization axis.

frequencies shown in the figure. Photon selections rules for this contribution imply that the $A^1\Sigma^+$-$b^3\Pi_0$ system does not contribute. Finally, we observe that the sum of Raman rates to vibrational levels $v'\neq 0$ of the $X^1\Sigma^+$ state is ten times smaller than the Raman rate to the $v'=0, J'=2$ rotational level of the $X^1\Sigma^+$ state (except where these rates are very small not shown in the figure.)

We plot total Raman rate

$$\gamma^{\rm Raman}_{{\rm X},vJM,{\rm tot}} = \sum_{v'J'\neq vJ}\sum_{M'}\gamma_{{\rm X},v'J'M'\leftarrow{\rm X},vJM} \tag{13}$$

and total Rayleigh rate

$$\gamma^{\rm Rayleigh}_{{\rm X},vJM,{\rm tot}} = \sum_{M'}\gamma_{{\rm X},vJM'\leftarrow{\rm X},vJM} \tag{14}$$

for the $v=0, J=0$ and $v=0, J=1$ rovibrational levels of the $X^1\Sigma^+$ state of $^{23}Na^{87}Rb$ in figure 6 as functions of laser frequency near the transition from the $v=0, J=0$ $X^1\Sigma^+$ state and the $v''=0, J''=1$ level of the coupled $A^1\Sigma^+$-$b^3\Pi_0$ system using a linear polarized laser photon along the z axis. The Raman and Rayleigh rates are independent of the sign of projection quantum number M. For the $v=0, J=0$ level the Raman rate is mostly smaller than the Raman rate, while for the $v=0, J=1$ level these ratios depends on projection quantum number M. The $v=0, J=1, M=\pm1$ rates are maximal for photon energy $\mathcal{E}_{v=0}+2B_{v=0}$, ignoring

the small difference between the rotational constants of the $v=0$ level of the $X^1\Sigma^+$ state and the $v''=0$ level of the coupled $A^1\Sigma^+$-$b^3\Pi_0$ system. The $v=0, J=1, M=0$ rates are maximal for photon energies $\mathcal{E}_{v=0}-4B_{v=0}$ and $\mathcal{E}_{v=0}+2B_{v=0}$ again ignoring the small differences in rotational constants. The two photon energies correspond to the $J''=0$ and 2 rotational states of $v''=0$ level of the coupled $A^1\Sigma^+$-$b^3\Pi_0$ system.

Finally, we observed that the Raman and Rayleigh rates are smallest near detunings of $h\times 90$ GHz to the blue of the transition between $v=0, J=0$ $X^1\Sigma^+$ state and the $v''=0, J''=1$ level of the coupled $A^1\Sigma^+$-$b^3\Pi_0$ system. This detuning is close to the detuning for the magic conditions discussed in figure 3. In fact, we find that for detunings near the magic conditions the ratio of $\gamma^{\rm Raman}/(2\pi I)$ and polarizability α for $v=0, J=0$ and $v=0, J=1$ is on the order of 10^{-6}. In other words, magic frequencies are also close to 'magic' for decoherences.

6. Conclusion

In this paper we have described theoretical calculations to characterize optical traps for a single NaRb molecule, where molecular rotational states have so called magic conditions. Constructing a rotational magic trap is the ideal solution to realize the long rotational coherence times needed to use rotational degrees of freedom as the quantum bit in quantum information processing. In such a laser trap, light-induced energy shifts of multiple rotational states of the ground configuration are (nearly) the same, eliminating dephasing associated with spatial variations in intensity across the trap. This might also open up the prospect of using the rotational degree of freedom of the molecule to encode a synthetic dimension in addition to having multiple molecule-containing traps in real space.

We reached this goal by changing the trapping laser frequency in a region that is close to or in between the narrow transitions from $v=0, J=0$ of the $X^1\Sigma^+$ state to the $v'=0$ and $v'=1$ vibrational levels of the spin-orbit coupled $A^1\Sigma^+$-$b^3\Pi_0$ complex. No external electric field is present while the magnetic field strength is 335.6 G. We predict nearly magic conditions for the lowest six rotational states of the $v=0$ level at detuning $\Delta/h=-2$ GHz and 100 GHz from the $v'=0, J'=1$ level of the $b^3\Pi_0$ potential. We have accounted for the nonzero nuclear spins of ^{23}Na and ^{87}Rb, which are aligned by the magnetic field through the Zeeman interaction. Finally, we have calculated Raman and Rayleigh scattering rates in the off-resonant absorption of a laser photon by the alkali-metal molecule and we realized that these rates are smallest for laser frequencies where magic conditions hold near detunings of 100 GHz.

Data availability statement

All data that support the findings of this study are included within the article (and any supplementary files).

Acknowledgments

Our research is supported by the U.S. Air Force Office of Scientific Research Grants No. FA9550-19-1-0272. Work at Temple University is also supported by the U.S. Air Force Office of Scientific Research Grants No. FA9550-21-1-0153 and the NSF Grant No. PHY-1908634.

ORCID iDs

Svetlana Kotochigova https://orcid.org/0000-0003-0580-3788
Eite Tiesinga https://orcid.org/0000-0003-0192-5585
Bryce Gadway https://orcid.org/0000-0003-3290-1850

References

[1] Kotochigova S and Tiesinga E 2006 Controlling polar molecules in optical lattices *Phys. Rev.* A **73** 041405(R)
[2] Neyenhuis B, Yan B, Moses S A, Covey J P, Chotia A, Petrov A, Kotochigova S, Ye J and Jin D S 2012 Anisotropic polarizability of ultracold polar ^{40}K^{87}Rb molecules *Phys. Rev. Lett.* **109** 230403
[3] Park J W, Yan Z Z, Loh H, Will S A and Zwierlein M W 2017 Second-scale nuclear spin coherence time of ultracold ^{23}Na^{40}K molecules *Science* **357** 372–5
[4] Seeßelberg F, Luo X-Y, Li M, Bause R, Kotochigova S, Bloch I and Gohle C 2018 Extending rotational coherence of interacting polar molecules in a spin-decoupled magic trap *Phys. Rev. Lett.* **121** 253401
[5] Kotochigova S and DeMille D 2010 Electric-field-dependent dynamic polarizability and state-insensitive conditions for optical trapping of diatomic polar molecules *Phys. Rev.* A **82** 063421
[6] Guan Q, Cornish S L and Kotochigova S 2021 Magic conditions for multiple rotational states of bialkali molecules in optical lattices *Phys. Rev.* A **103** 043311
[7] He J, Lin J, Vexiau R, Bouloufa-Maafa N, Dulieu O and Wang D 2021 Characterization of the lowest electronically excited-state ro-vibrational level of ^{23}Na^{87}Rb *New J. Phys.* **23** 115003

[8] Ni K-K, Ospelkaus S, de Miranda M H G, Pe'er A, Neyenhuis B, Zirbel J J, Kotochigova S, Julienne P S, Jin D S and Ye J 2008 A high phase-space-density gas of polar molecules in the rovibrational ground state *Science* **322** 231
[9] Bause R, Li M, Schindewolf A, Chen X-Y, Duda M, Kotochigova S, Bloch I and Luo X-Y 2020 Tune-out and magic wavelengths for ground-state ^{23}Na^{40}K molecules *Phys. Rev. Lett.* **125** 023201
[10] Gregory P D, Fernley L M, Tao A L, Bromley S L, Stepp J, Zhang Z, Kotochigova S, Hazzard K R A and Cornish S L 2024 Second-scale rotational coherence and dipolar interactions in a gas of ultracold polar molecules *Nat. Phys.* **20** 415
[11] Lin J, He J, Ye X and Wang D 2021 Anisotropic polarizability of ultracold ground-state ^{23}Na^{87}Rb molecules *Phys. Rev.* A **103** 023332
[12] Zhu B, Li X, He X, Guo M, Wang F, Vexiau R, Bouloufa-Maafa N, Dulieu O and Wang D 2016 Long-range states of the NaRb molecule near the Na$(3^2S_{1/2})$ + Rb$(5^2P_{3/2})$ asymptote *Phys. Rev.* A **93** 012508
[13] Cline R A, Miller J D, Matthews M R and Heinzen D J 1994 Spin relaxation of optically trapped atoms by light scattering *Opt. Lett.* **19** 207–9
[14] Uys H, Biercuk M J, VanDevender A P, Ospelkaus C, Meiser D, Ozeri R and Bollinger J J 2010 Decoherence due to elastic Rayleigh scattering *Phys. Rev. Lett.* **105** 200401
[15] Brown N C and Brown K R 2018 Comparing Zeeman qubits to hyperfine qubits in the context of the surface code: ^{174}Yb$^+$ and ^{171}Yb$^+$ *Phys. Rev.* A **97** 052301
[16] Herzberg G 1950 *Spectra of Diatomic Molecules* 2nd edn (D. van Nostrand Company, Inc.)
[17] Docenko O, Tamanis M, Ferber R, Pazyuk E A, Zaitsevskii A, Stolyarov A V, Pashov A, Knöckel H and Tiemann E 2007 Deperturbation treatment of the $A^1\Sigma^+ - b^3\Pi$ complex of NaRb and prospects for ultracold molecule formation in $X^1\Sigma^+(v = 0; j = 0)$ *Phys. Rev.* A **75** 042503
[18] Pashov A, Docenko O, Tamanis M, Ferber R, Knöckel H and Tiemann E 2005 Potentials for modeling cold collisions between Na(3S) and Rb(5S) atoms *Phys. Rev.* A **72** 062505
[19] Shao Y *et al* 2015 Advances in molecular quantum chemistry contained in the Q-Chem 4 program package *Mol. Phys.* **113** 184–215
[20] Colbert D T and Miller W H 1992 A novel discrete variable representation for quantum mechanical reactive scattering via the S-matrix Kohn method *J. Chem. Phys.* **96** 1982–91
[21] Borsalino D Vexiau R, Lepers M, Orbán A, Aymar M, Dulieu O and Bouloufa-Maafa N 2017 Dynamic dipole polarizabilities of heteronuclear alkali dimers: optical response, trapping and control of ultracold molecules *Int. Rev. Phys. Chem.* **36** 709–50
[22] Zygelman B and Dalgarno A 1988 Radiative quenching of He(2^1S) induced by collisions with ground-state helium atoms *Phys. Rev.* A **38** 1877–84
[23] Loudon R 2000 *The Quantum Theory of Light* 3rd edn (Oxford University Press)